PAPER

A comparison of sensitized Ln(III) emission using pyridine- and pyrazine-2,6-dicarboxylates†

Evan G. Moore*

The synthesis, X-ray structure, solution stability, and photophysical properties of Eu(III) complexes with pyrazine-2,6-dicarboxylic acid (H$_2$PYZ) are reported, and compared to structurally analogous complexes with pyridine-2,6-dicarboxylic acid (H$_2$DPA). The [Eu(PYZ)$_3$]$^{3-}$ complex demonstrates highly efficient metal-centered Eu(III) luminescence in the solid state ($\Phi_{total} \sim 60.9\%$). In aqueous solution, moderate stability is retained at pH 7.4 (pEu $\sim$ 10.5), although hydrolysis of the complex anion becomes competitive below mM concentrations, and the observed luminescence intensity from the Eu(III) metal ion is reduced as a result. A complete evaluation of the thermodynamic solution stability has allowed the observed differences in the solution behaviour luminescence properties of these complexes to be rationalized. An analysis of their luminescence behaviour in the solid state has also allowed a direct comparison of the sensitisation behaviour for these isostructural compounds.

Introduction

The use of trivalent lanthanide complexes with Eu(III) and Tb(III) has undergone a surge of renewed interest, in particular due to their use in biotechnology. These emissive optical probes can be used to gain a more detailed understanding of structure–function relationships in biological systems,[1] and have been developed for the detection of several important biomolecules.[2,3] Emissive Ln(III) cations are particularly suitable for this task since they are relatively insensitive to quenching by molecular oxygen, they possess sharp and characteristic emission spectra, and they demonstrate large 'effective' Stokes shifts (*i.e.* the difference between excitation and emission wavelengths). Moreover, their long-lived luminescent lifetimes allow for both spectral and time-resolved discrimination of the luminescent signal. In this way, their emission can be readily distinguished from that of short-lived organic fluorophores and background autofluorescence using time-gating techniques, resulting in overall improved sensitivity.[4]

Not surprisingly, there have been numerous examples of luminescent Ln(III) complexes reported in the literature, with emission spanning from the visible[5–7] to near-infra red (NIR) regions.[8,9] A common feature for these systems is the use of an organic chromophore, which either incorporates a donor atom (or atoms) capable of forming coordinate bonds to the lanthanide cation, or that is otherwise covalently linked to a metal-binding component, resulting in thermodynamically stable complexes. This chromophore then functions as an 'antenna', absorbing incident photons and transferring this electronic excitation to the metal, which is necessary since the direct 4f–4f absorptions of Ln(III) cations are Laporte forbidden, and hence very weak. The overall luminescence quantum yield for the complex, Φ_{total}, is thus dependent on η_{sens}, the efficiency of this sensitization process, and Φ_{Ln}, the intrinsic metal-centered quantum yield of the metal; $\Phi_{total} = \eta_{sens}\Phi_{Ln}$. As is often the case, if sensitization is assumed to proceed *via* the lowest energy T$_1$ triplet state of the ligand, then the sensitization efficiency is a function of Φ_{isc}, the quantum yield for intersystem crossing, and η_{eet}, the efficiency of the ligand-to-metal energy transfer; $\eta_{sens} = \Phi_{isc}\eta_{eet}$.

Of the many antennae, pyridine-2,6-dicarboxylic acid or 'dipicolinic acid' (H$_2$DPA, Chart 1) is a well-known organic sensitizer for Eu(III) luminescence. The dipicolinate dianion, DPA^{2-}, reacts with Ln(III) cations to form mono, bis, and tris ligated complexes. The complex speciation has been well characterised[10] and the Tb(III) and Eu(III) complexes of this ligand have been proposed as useful standards for quantum yield determinations of Ln(III) complexes, with $\Phi_{total} = 24 \pm 2.5\%$ for 75 μM solutions of the Eu(III) complex.[10] For millimolar solutions, where the higher concentration leads to complex speciation which can be considered to be *ca.* 100% ML$_3$ complex, the
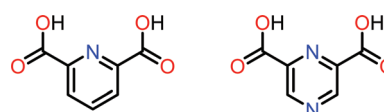
School of Chemistry, University of Melbourne, Parkville, VIC 3010, Australia. E-mail: egmoore@unimelb.edu.au; Fax: +61 (0) 3 9347 5180; Tel: +61 (0) 3 8344 5939
†Electronic supplementary information (ESI) available: X-ray data in CIF format, additional figures and luminescence spectra. CCDC 862688. For ESI and crystallographic data in CIF or other electronic format see DOI: 10.1039/c2dt30062a

Chart 1 Chemical structures of H$_2$DPA (left) and H$_2$PYZ (right) ligands.

reported[11] quantum yield in aqueous solution is as high as $\Phi_{total} = 29\% \pm 2\%$ for $[Eu(DPA)_3]^{3-}$.

We noted previous reports[12] that have shown the S_1 (n–π*) excited state of the pyrazine chromophore has a much higher intersystem crossing quantum yield ($\Phi_{isc} \sim 1.0$) when compared to pyridine ($\Phi_{isc} \sim 0.3$), and rationalized the Eu(III) complexes of pyrazine-2,6-dicarboxylic acid (H$_2$PYZ, Chart 1) may show improved luminescence performance. This ligand has been used previously[13] with Ln(III) cations to prepare novel 3d–4f coordination polymers with interesting architectures, however, a detailed examination of its photophysical properties with Eu(III) has not been reported. Herein, we report the synthesis, structure, stability, and photophysical properties of Eu(III) complexes with the pyrazine-2,6-dicarboxylate dianion (PYZ^{2-}). The luminescence properties of this complex have been evaluated in buffered aqueous solution (pH 7.4) and in the solid state, showing particularly efficient metal centered emission in the latter case.

Experimental

General

All solvents for reactions were dried using standard methodologies. Pyridine-2,6-dicarboxylic acid (H$_2$DPA), high purity Eu$_2$O$_3$ (>99.99%), and Cs$_2$CO$_3$ were used as supplied by Sigma Aldrich (Castle Hill, Australia). Cs$_3$[Eu(DPA)$_3$]·9H$_2$O was prepared using literature methods.[16] ^{1}H and ^{13}C NMR spectra were obtained using a Varian Unity 400 MHz spectrometer, and chemical shifts are reported in ppm relative to TMS. Elemental analyses were performed by Microanalytical Services at the School of Chemistry and Molecular Biosciences, University of Queensland, Australia.

Synthesis

Pyrazine-2,6-dicarboxylic acid (H$_2$PYZ). This ligand was prepared using literature methods,[14,15] starting from 1.0 g (4.6 mmol) of pyrazine-2,3,5-tricarboxylic acid. After selective decarboxylation, the desired isomer was recrystallised from water, yielding 442 mg (2.2 mmol, 46%) of colorless needles (m.p. 224 °C). ^{1}H NMR (400 MHz, D$_2$O/NaOD): δ = 8.64 (s, 2 H) ppm. ^{13}C NMR (100.6 MHz, D$_2$O/NaOD): δ = 146.4, 149.1, 190.0 ppm. Anal. calcd (found) for C$_6$H$_4$N$_2$O$_4$·2H$_2$O (mol. wt = 204.14 g mol^{-1}): C, 35.30 (35.35); H, 3.95 (3.84); N, 13.72 (13.66).

Cs$_3$[Eu(PYZ)$_3$]·7H$_2$O. A suspension of Eu$_2$O$_3$ (60 mg, 0.17 mmol) and H$_2$PYZ (168 mg, 1 mmol) in water (10 mL) was heated to *ca.* 80 °C with stirring for 1 hour, followed by the addition of solid Cs$_2$CO$_3$ (*ca.* 170 mg, 0.5 mmol) until the pH was *ca.* 6.0. The resulting solution was allowed to cool to room temperature, filtered, and then evaporated to dryness *in vacuo*, giving a white solid which was recrystallised by dissolving in the minimum volume of hot MeOH, yielding a microcrystalline solid which was collected by vacuum filtration (349 mg, 88% yield). Anal. calcd (found) for Cs$_3$EuC$_{18}$H$_6$N$_6$O$_{12}$·7H$_2$O (mol. wt = 1193.09 g mol^{-1}): C, 18.40 (18.00); H, 1.72 (1.78); N, 7.15 (7.02). X-ray quality crystals were obtained by slow evaporation of the filtrate.

X-ray crystallography

X-ray crystallographic data for Cs$_3$[Eu(PYZ)$_3$]·7H$_2$O was measured using an Oxford dual source SuperNova Diffractometer with Atlas CCD detector, employing graphite-monochromated Mo K$_\alpha$ radiation (0.71073 Å). Single crystals were coated in Paratone-N oil and mounted on a cryo loop for data collection, with external cooling at 130 K provided by an Oxford Cryostream LT device. Empirical absorption corrections were performed using a multifaceted crystal model and the ABSPACK routine within the CrysAlisPro software package. The structure was solved by direct methods and refined by the full-matrix least-squares method on F^2 with SHELXL-97,[17] using the WinGX software package.[18]

The crystals obtained were generally of poor quality, showing evidence of merohedral twinning and disorder. After several attempts, a single crystal was selected for data collection that showed only a small amount of disorder. Our attempts to model this disorder were unsuccessful, with a calculated occupancy factor of only *ca.* 3%, and the resulting refinements became unstable. Accordingly, refinement was continued with all atoms assigned full occupancies (or 0.5 for those on special positions). However, after assigning all atoms, the residual electron density map showed anomalous peaks of 2–3.5 e Å^{-3}, which were related by 0.5,0,0 to the coordinates of the assigned heavy atoms. As these residual electron density peaks were close to several atoms of the ligand, the anisotropic displacement parameters for these atoms were constrained to near isotropic values. All other non-H atoms were refined anisotropically. The H atoms of the pyrazine ligand and coordinated water molecules were positioned geometrically and refined using a riding model, with $U_{iso}(H) = 1.2U_{eq}(C/O)$. Diagrams of the resulting structure were created using the Mercury software package.[19]

Photophysics

Typical solution concentrations for absorption and fluorescence measurements were *ca.* 10^{-5} to 10^{-6} M and 1.0 cm cells in quartz suprasil were used. UV-Visible absorption spectra were recorded with a Varian 50 double beam absorption spectrometer. Emission spectra were acquired with a HORIBA Jobin Yvon IBH FluoroLog-311 spectrofluorimeter. Spectra were reference corrected for both the excitation light source variation (lamp and grating) and the emission spectral response (detector and grating). Absolute quantum yields in the solid state were determined using an integrating sphere, with solid samples dispersed in KBr as an optically transparent host matrix, and a literature value[20] of $\eta = 1.57$ for the refractive index. Quantum yields in solution were determined by the optically dilute method[21] using the following equation:

$$\frac{\Phi_x}{\Phi_r} = \left[\frac{A_r(\lambda_r)}{A_x(\lambda_x)}\right]\left[\frac{I(\lambda_r)}{I(\lambda_x)}\right]\left[\frac{\eta_x^2}{\eta_r^2}\right]\left[\frac{D_x}{D_r}\right]$$

where A is the absorbance at the excitation wavelength (λ), I is the intensity of the excitation light at the same wavelength, η is the refractive index and D is the integrated luminescence intensity. The subscripts 'x' and 'r' refer to the sample and reference respectively. A methanol solution of cresyl violet perchlorate was

used as the reference ($\Phi_r = 0.54$).[22] The estimated error for these measurements is ±15%.[22]

Time-resolved experiments were performed using a nanosecond laser setup. The tripled output of a Q-switched Nd:YAG (Continuum NY-61-10, Coherent) at 355 nm and 10 Hz was used to drive an OPO system (Casix BBO, Shanghai Uniwave Technologies) tuned to 560 nm, which was then frequency doubled using a type-1 BBO crystal to afford excitation pulses at 280 nm. These were focused on the sample using all quartz optics, and the emission from the sample was collected perpendicular to the excitation beam, collimated then refocused onto the entrance port of a 0.3 m triple grating monochromator (SpectraPro 300i, Acton Instruments). The detector was a standard photomultiplier tube (R928P, Hamamatsu) operating at −800 V, which was sampled directly using a 500 MHz digital oscilloscope (TDS520, Tektronix) using the sync out signal from the Q-switched Nd:YAG as the trigger. The instrument response function (IRF) for this experimental setup was measured to be *ca.* 12 ns at FWHM using scattered excitation from a Ludox solution. Data analysis was performed using a commercially available software package (Igor, Version 6.1.2.1, Wavemetrics). Each trace contained at least 500 data points and was averaged over 1000 shots. The quality of the fit was assessed using the calculated reduced chi-squared χ^2 function and by a visual inspection of the weighted residuals. The estimated error for these measurements is ±10%.[22]

Solution thermodynamics

Potentiometric titrations were performed under N_2 atmosphere in aqueous solutions prepared from Millipore water (18.2 MΩ cm resistivity) containing 0.1 M Et_4NClO_4. Temperature control at 25 ± 0.1 °C was achieved using a thermostatted titration vessel with an external circulating water bath, and titrant addition in 3–6 μL aliquots was automated using a Metrohm 796 titroprocessor. Calibration of the combined pH glass electrode was performed by strong acid titration of standardised 6 mM aqueous $HClO_4$ with *ca.* 0.1 M Et_4NOH, and resulting potentiometric data was analysed using GLEE[23] with a fixed ionic product for water of $pK_w = 13.78$ at 25 °C and $I = 0.1$ M.

Ligand pK_a's were determined by continuous potentiometric titration of 25.0 mL solutions of *ca.* 6 mM aqueous $HClO_4$ containing *ca.* 1.13 mM of the ligand *versus ca.* 0.1 M Et_4NOH. The resulting potentiometric data (pH *vs.* vol. OH^- added) for four independent experiments were analysed globally using Hyperquad.[24] The initial concentration of ligand was held fixed in the refinement.

Corresponding formation constants with Eu(III) were also determined by continuous potentiometric titration after the addition of aliquots of $Eu(ClO_4)_3$ to obtain 1.25 : 1, 2.75 : 1, and 4 : 1 ligand-to-metal stoichiometry. A solution of $Eu(ClO_4)_3$ with accurately known concentration was prepared from 99.99% Eu_2O_3 (Aldrich) and 70% $HClO_4$ using literature methodology,[25] then subsequently diluted to a known volume with *ca.* 6 mM aqueous $HClO_4$ in 0.1 M Et_4NClO_4. The resulting potentiometric data (pH *vs.* vol. OH^{-1} added) for seven independent experiments were analysed globally using Hyperquad.[24] For M : L stoichiometries of less than 1 : 3, the data above *ca.* pH 6

Table 1 Summary of X-ray crystal data for $Cs_3[Eu(PYZ)_3]\cdot7H_2O$

Formula	$C_{18}H_{20}N_6O_{19}Cs_3Eu$
Formula weight/g mol^{-1}	1175.09
Crystal system	Hexagonal
Space group	$P6_122$
a/Å	10.4302(2)
c/Å	55.1896(13)
V/Å^3	5199.64(19)
Z	6
T/K	130
ρ_{calc}/g cm^{-3}	2.252
μ/mm^{-1}	4.996
Reflns measured	22 222
Unique reflns	4070
Data/ restraints/ parameters	4070/48/214
R_{int}	0.0449
R_1 [$I > 2\sigma(I)$]	0.0865
wR_2 (all data)	0.2083
Goodness-of-fit on F^2	1.311
$\Delta\rho_{max,min}$/e Å^{-3}	3.604, −2.458

was discarded due to visible evidence of insoluble Eu(hydroxo) species formation. The initial concentrations of ligand and metal were fixed in the refinement, together with the ligand pK_a values. Hydrolysis constants for Eu(III) were also included in the model ($\beta_{10-1} = -7.1$, $\beta_{10-2} = -15.6$, $\beta_{10-3} = -24.6$, and $\beta_{10-4} = -34.81$), which were calculated using the methods described in Baes and Mesmer[26] for an ionic strength of $I = 0.1$ M.

Results and discussion

Synthesis and structure

The synthesis of the bis-heteroarene ligand, pyrazine-2,6-dicarboxylic acid (H_2PYZ), has been previously reported[14,15] *via* selective decarboxylation of pyrazine-2,3,5-tricarboxylic acid, and the $[Eu(PYZ)_3]^{3-}$ complex was readily prepared by gentle heating of this ligand and europium oxide in aqueous solvent, using caesium carbonate as a base. The resulting complex was isolated in analytically pure form as the hydrated tris caesium salt, and X-ray quality crystals of the Eu(III) complex were grown by slow evaporation of the complex from a methanol solution.

The $Cs_3[Eu(PYZ)_3]\cdot7H_2O$ complex crystallized in the $P6_122$ space group with primitive hexagonal Bravais lattice, and a full summary of the crystallographic and structure refinement details is given in Table 1. The presence of structural disorder and merohedral twinning complicated the data refinement. However, after several attempts, a single crystal was selected for data collection that showed only a small amount of disorder, and a resulting structure solution was obtained, clearly showing the connectivity of the complex. A view of the resulting unit cell contents and the complex anion are shown in Fig. 1.

The expected tridentate coordination mode of the PYZ^{2-} dianion with Eu(III) is observed, with a tricapped trigonal prismatic geometry at the metal centre, approximating D_3 symmetry (Fig. 1b), commonly observed for nine-coordinate (CN = 9) Ln(III) complexes. Within the asymmetric unit, the Eu, N3 and N4 atoms lie on a 2-fold proper rotation axis, and each possess half occupancy. The three coordinating pyrazine nitrogen atoms that result (N1 × 2, and N3) form a plane perpendicular to the
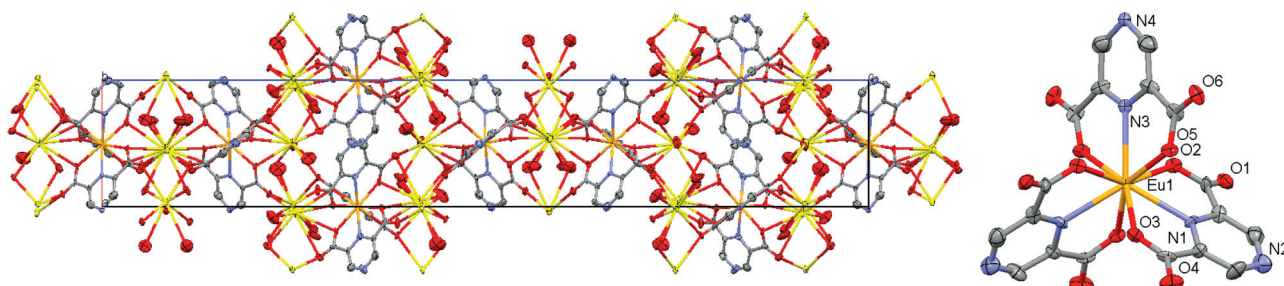
Fig. 1 (a) A view of the X-ray crystal structure for $Cs_3[Eu(PYZ)_3] \cdot 7H_2O$ along the b-axis showing unit cell contents (left) and (b) a view of the complex anion down the molecular C_3 axis (right) with selected atom labels (C, grey; O, red; N, blue; Eu, orange; Cs, yellow, 50% probability ellipsoids shown). Caesium counter cations and solvent H_2O molecules removed for clarity in (b).

crystallographic c axis (and molecular C_3 axis). The coordination sphere of the Eu(III) cation is completed by two coordinated carboxylate oxygen atoms from each of the three ligands which form two trigonal faces, resulting in upper and lower basal planes defined by the O5, O2 and O3 atoms which are approximately parallel ($\angle 1.1°$). A small distortion of the idealized D_3 symmetry arises *via* a rotation of the trigonal faces thus formed by *ca.* 17° with respect to each other about the molecular C_3 axis. The two unique Eu–N bond lengths (Eu1–N1 and Eu1–N3) are almost identical at 2.53 Å and 2.56 Å respectively, while the coordinate oxygen bond lengths (Eu1–O2 = 2.43 Å, Eu1–O5 = 2.47 Å, Eu1–O3 = 2.47 Å) are slightly shorter.

The overall trianionic charge of the complex anion was confirmed by the presence of the requisite number of Cs^+ counter cations, which form an extended polymeric network by coordinate interactions with several bridging water and carboxylate oxygen atoms. For Cs1, which lies along the 6-fold screw axis (c axis) and has half occupancy, the alkali metal is eight coordinate (CN = 8), with four oxygen donor atoms originating from two symmetry related bridging water molecules (O8 × 2 and O7 × 2) and the remaining donor atoms from the carboxylic acid groups of the PYZ^{2-} ligands (O6 × 2 and O4 × 2). For Cs2, the metal is also eight coordinate, with two donor oxygen atoms from bridging water molecules (O7 and O8), five from carboxylic acid groups of the PYZ^{2-} ligand (O1, O2, O3, O5 and O6) and a single non-bridging water molecule (O9). A single non-coordinated water molecule (O10) completes the asymmetric unit, and also forms strong H bonding interactions with H7B (O10···H7B–O7 = 2.47 Å) and H9A (O10···H9A–O9 = 2.43 Å).

The structure of $Cs_3[Eu(PYZ)_3] \cdot 7H_2O$ shares considerable similarities with that reported[16] for $Cs_3[Eu(DPA)_3] \cdot 9H_2O$. In both cases, the structures can be considered to be built up of successive anionic Ln(III) complex/cationic Cs^+ layers which extend along the crystallographic c-axis. However, in the present case, the positions of the Eu(III) metal centers are offset by a translation of half a unit cell in every third layer (see Fig. S1, ESI†). Nonetheless, the shortest Eu···Eu separations between adjacent complexes are almost equivalent, at 10.41 Å for $Cs_3[Eu(DPA)_3] \cdot 9H_2O$ *versus* 10.54 Å for $Cs_3[Eu(PYZ)_3] \cdot 7H_2O$, while the closest Eu···Cs distances are 4.58 Å and 4.52 Å respectively. Indeed, the only major difference we note is the presence of a single lattice water molecule in the present case, compared to two in the reported[16] structure of $Cs_3[Eu-$
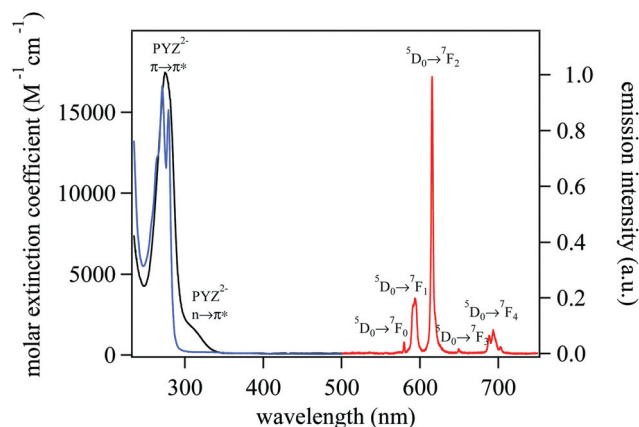

Fig. 2 UV-Visible absorption spectra of $[Eu(DPA)_3]^{3-}$ (blue) and $[Eu(PYZ)_3]^{3-}$ (black) complexes and corresponding emission spectrum (red, λ_{ex} = 275 nm) of $[Eu(PYZ)_3]^{3-}$ in 0.1 M HEPES buffer at pH 7.4.

$(DPA)_3] \cdot 9H_2O$, which may be due to slightly more efficient packing of the pyrazine complex.

Aqueous stability and photophysics

The absorption spectrum for the $[Eu(PYZ)_3]^{3-}$ complex in 0.1 M HEPES buffer at pH 7.4 is shown in Fig. 2, and is characterised by a broad absorption band at *ca.* 274 nm ($\varepsilon = 17\,360\ M^{-1}$ cm^{-1}), with a less intense shoulder at *ca.* 308 nm ($\varepsilon = 1670\ M^{-1}$ cm^{-1}). On the basis of previous work,[12] we assign these bands to the $S_0 \rightarrow S_2$ and $S_0 \rightarrow S_1$ transitions of the coordinated PYZ^{2-} chromophore, with principally $\pi \rightarrow \pi^*$ and $n \rightarrow \pi^*$ character respectively. In comparison to the spectrum of $[Eu(DPA)_3]^{3-}$, we note the emergence of this new $n \rightarrow \pi^*$ band also coincides with a loss of the otherwise well-resolved vibrational structure, as displayed by the coordinated DPA^{2-} dianion. Also shown in Fig. 2 is the corresponding emission spectra for the $[Eu(PYZ)_3]^{3-}$ complex, which displays typical metal centered Eu(III) transitions from the $^5D_0$ excited state to the ground state ^7F_J manifold. Peak maxima are apparent at *ca.* 580 ($J = 0$), 593 ($J = 1$), 615 ($J = 2$), 649 ($J = 3$) and 688, 693, 703 nm ($J = 4$). In comparison to the spectrum of the $[Eu(DPA)_3]^{3-}$ anion, we also particularly note that the $^5D_0 \rightarrow {}^7F_0$ transition for the $[Eu(PYZ)_3]^{3-}$ complex is much more clearly evident (accounting for *ca.* 1% of the total

Table 2 Summary of absorption and luminescence properties for solutions of the $[Eu(PYZ)_3]^{3-}$ and $[Eu(DPA)_3]^{3-}$ complexes in 0.1 M HEPES buffer at pH 7.4

Complex	λ_{max} (nm)	ε_{max} (M^{-1} cm^{-1})	Φ_{total} [a] (%)	τ_{obs} [b] (H$_2$O) (ms)	τ_{obs} [b] (D$_2$O) (ms)	q (± 0.5)
$[Eu(PYZ)_x]$	274	17 360	4.3	1.42 (15%)	2.31 (100%)	0.3
(x = 3, 2, 1)	308[c]	1670		0.34 (85%)		2.6
$[Eu(DPA)_x]$	271	16 560	9.1	1.64 (80%)	3.04 (100%)	0.3
(x = 3, 2, 1)	279	15 090		0.31 (20%)		2.9

[a] Measured using *ca.* 2–6 μM solutions *vs.* cresol violet ClO$_4$ in MeOH, Φ_{ref} = 0.54. [b] Measured using 50 μM solutions. [c] Shoulder.
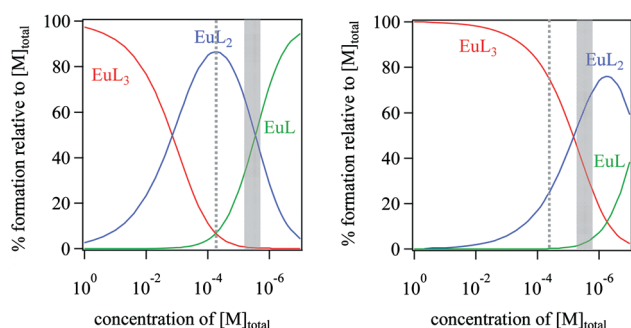

Fig. 3 The calculated speciation *versus* concentration for $[Eu(PYZ)_3]^{3-}$ (left) and $[Eu(DPA)_3]^{3-}$ (right) complexes upon dilution at pH = 7.4 (right). Concentrations used for τ_{obs} (*ca.* 50 μM) and Φ_{total} (*ca.* 2–6 μM) measurements are indicated by the grey dashed lines and grey shaded areas (see text).

integrated luminescence signal) and the $^5D_0 \rightarrow {}^7F_1$ transition of the $[Eu(PYZ)_3]^{3-}$ complex is broader, and less clearly resolved (see Fig. S2, ESI†).

To further elucidate the photophysical properties, we have undertaken quantitative analysis of the observed Eu(III) centered emission, measuring the overall metal-centered luminescence quantum yield, Φ_{total}, using cresol violet perchlorate in MeOH (Φ_{ref} = 0.54) as a suitable quantum yield standard.[22] The resulting data (see Fig. S3, ESI†) is summarised in Table 2, where we note that the anticipated enhancement in Φ_{total} was not realised. Moreover, the quantum yield is less than half the value for the analogous $[Eu(DPA)_3]^{3-}$ complex of when measured under identical conditions. We note that our Φ_{total} values for solutions of the $[Eu(DPA)_3]^{3-}$ complex are lower than those previously reported[10,11] by Bünzli *et al*. This is due to the lower concentrations utilised in our experiments (*e.g.* 2–6 μM), which leads to substantial hydrolysis of the ML$_3$ complex, as shown in Fig. 3, and therefore a decrease in the observed quantum yield upon dilution is to be expected.

We have also determined the time resolved decay profiles for the $^5D_0 \rightarrow {}^7F_2$ transition at *ca.* 615 nm for *ca.* 50 μM solutions of both compounds. While both decays were clearly biexponential, for the $[Eu(PYZ)_3]^{3-}$ complex, the major contributor (>80%) towards the biexponential decay has a much shorter lifetime, at 0.34 ms. Corresponding measurements in D$_2$O confirmed that the major species present in solution was indeed the $[Eu(PYZ)_2(H_2O)_q]^{3-}$ complex, with a value for 'q', the total

number of inner sphere water molecules, calculated to be 2.6 ± 0.5 from the well known Horrocks relationship.[27] For the Eu(III) complexes with DPA^{2-}, by contrast, the $[Eu(DPA)_3]^{3-}$ species remains predominant in solution at these concentrations, with a smaller amount of the $[Eu(DPA)_2(H_2O)_q]^{3-}$ species formation.

In order to confirm the photophysical behaviour observed in aqueous solution, it was necessary to determine the protonation and aqueous stability constants for the H$_2$PYZ ligand and its Eu(III) complexes using potentiometric techniques. Within the pH range studied (*ca.* 2.2–11.3), two protonation constants for the ligand were identified, with values of $\log_{10} \beta_{011}$ = 3.34 (2) (= pK_{a2}) and $\log_{10} \beta_{012}$ = 5.15 (3) (pK_{a1} = 1.81) in 0.1 M Et$_4$NClO$_4$, which we assign to sequential protonation of the carboxylic acid groups. These values are consistent with the pK_a's reported by Lewis[28] of 3.53 and 2.35 for the same ligand, measured in the absence of supporting electrolyte. Overall, the H$_2$PYZ ligand can be considered to be slightly more acidic than the corresponding H$_2$DPA analogue, with reported[30] values of pK_{a2} = 4.76 and pK_{a1} = 2.16.

The formation constants with Eu(III) were also determined potentiometrically, and the resulting values are summarised in Table 3. The most satisfactory fit of the titration data was obtained using a model with three successive $\log_{10} \beta_{MLH}$ formation constants where the subscripts define the product stoichiometry, β_{MLH} = ($[M_ML_LH_H]/[M]^M[L]^L[H]^H$) and, in this case, correspond to formation of the M + L $\rightleftharpoons$ ML, M + 2L $\rightleftharpoons$ ML$_2$, and M + 3L $\rightleftharpoons$ ML$_3$ complexes respectively, where L is the PYZ^{2-} dianion. This model indicates an absence of competing protonation equilibria involving the 'free' pyrazine nitrogens of the metal complex, which have very poor basicity. A comparison of the resulting Eu(III) complex formation constants between H$_2$PYZ and the analogous H$_2$DPA ligand reveals that the pyrazine derivative, overall, forms weaker complexes in aqueous solution with Eu(III), resulting in a three order of magnitude difference between the $\log_{10} \beta_{130}$ values. We ascribe this difference to the poorer donating ability of the electron-deficient pyrazine *versus* pyridine nitrogen atom. Indeed, previous work with multidentate chelates has shown that pyrazine N atoms are much softer donors, and contribute very little to resulting lanthanide complex stabilities.[31] Interestingly, the $\log_{10} \beta_{110}$ values are quite similar for the two ligands, underlining the essentially electrostatic interaction between the hydrated trivalent lanthanide cation and dianionic ligand especially in the first complexation step. The slightly larger value we observe for $\log_{10} \beta_{110}$ with H$_2$PYZ is likely an artifact due to our use of a less-coordinating supporting electrolyte system (Me$_4$NClO$_4$ *versus* KCl) compared to the literature values.

The resulting concentration dependence of complex speciation is shown in Fig. 3, where it is readily apparent that, as a result of the decreased complex stability, the $[Eu(PYZ)_3]^{3-}$ complex dissociates in aqueous solution upon dilution much more rapidly than the corresponding $[Eu(DPA)_3]^{3-}$ analogue, and below *ca.* mM concentrations a significant amount of the $[Eu(PYZ)_2(H_2O)_x]^-$ complex is formed.

These differences in solution speciation between the $[Eu(PYZ)_3]^{3-}$ and $[Eu(DPA)_3]^{3-}$ complexes have a dramatic influence on the photophysical properties discussed herein (*vide supra*). For example, the larger intensity of the $^5D_0 \rightarrow {}^7F_0$

Table 3 Summary of ligand protonation and Eu(III) complex formation constants ($\log_{10} \beta_{MLH}$) for H$_2$PYZ in comparison to reported[29,30] literature values for H$_2$DPA

Ligand	$\log_{10} \beta_{011}$	$\log_{10} \beta_{012}$	$\log_{10} \beta_{110}$	$\log_{10} \beta_{120}$	$\log_{10} \beta_{130}$	pM^b
H$_2$PYZ	3.34 (2)	5.15 (3)	9.06 (5)	14.01 (13)	18.35 (16)	10.26
H$_2$DPA^a	4.76	6.92	8.84 (1)	15.98 (3)	21.49 (5)	12.23

^{a} Literature data taken from ref. 29 and 30. ^{b} pM = $-\log_{10}$ [M]$_{free}$ with [M]$_{total}$ = 10^{-6} M, [L]$_{total}$ = 10^{-5} M, pH = 7.4 (25 °C, 0.1 M Et$_4$NClO$_4$).

transition at *ca.* 580 nm for *ca.* 50 μM solutions of [Eu(PYZ)$_3$]$^{3-}$ can be rationalized by the presence of two emitting species in solution, with the ML$_2$ complex being predominant. For the same reason, the $^5D_0 \rightarrow {}^7F_1$ transition at *ca.* 590 nm also appears as a broader signal. The additional intensity observed for the $J = 0$ peak is likely due to the lower symmetry of the Eu(III) cation for the ML$_2$ complex, compared to the ML$_3$ (*e.g.* C_2 *vs.* D_3), since this electric dipole transition is known[32] to gain intensity through J mixing in lower symmetry environments. By contrast, for [Eu(DPA)$_3$]$^{3-}$, the aqueous speciation at 50 μM indicates that *ca.* 80% of the Eu(III) complex is present as the ML$_3$ species. We also note that the observed biexponential luminescence lifetimes for both the [Eu(PYZ)$_3$]$^{3-}$ and [Eu(DPA)$_3$]$^{3-}$ complexes are completely consistent with the solution thermodynamic model. The corresponding measurements in deuterated solvent, and hence estimates of the inner-sphere hydration number, q, allow us to confirm that the ML$_2$ species for both compounds contains three bound solvent water molecules, and hence take the form [Eu(L)$_2$(H$_2$O)$_3$]$^-$, where L = PYZ^{2-} or DPA^{2-}.

The Eu(III) centered luminescence quantum yield, Φ_{total}, was markedly lower for complexes with PYZ^{2-} compared to DPA^{2-}, as reported in Table 2. However, since these measurements were undertaken in dilute aqueous solutions (2–6 μM) in order to maintain an absorbance of less than 0.1, the complex speciation in Fig. 3 reveals that the predominant species in solution with the PYZ^{2-} ligand at these concentrations are in fact the ML$_2$ and ML complexes, with less than 1% of the intact ML$_3$ complex remaining. Due to the presence of inner-sphere water molecules on these hydrolyzed complexes, which have a well-known[33] quenching effect *via* non-radiative relaxation processes, the metal-centered luminescence is significantly reduced. Indeed, even in significantly more concentrated solutions, partial dissociation of the ML$_3$ complex will inevitably reduce the overall luminescence intensity compared to Eu(III) complexes with DPA^{2-}, which makes a direct comparison of the sensitisation efficiencies with these differing organic ligands problematic in aqueous solution.

Solid-state luminescence

In order to accurately compare the sensitisation behaviour of these two ligands, we have instead undertaken luminescence measurement in the solid state, using microcrystalline materials such that complex dissociation is no longer problematic. The observed excitation (λ_{em} = 615 nm) and emission (λ_{em} = 340 nm) spectra obtained for Cs$_3$[Eu(PYZ)$_3$]·7H$_2$O are shown in Fig. 4.

The latter shows easily recognisable peaks corresponding to transitions from the Eu(III) $^5D_0$ excited state to ground state ^7F_J
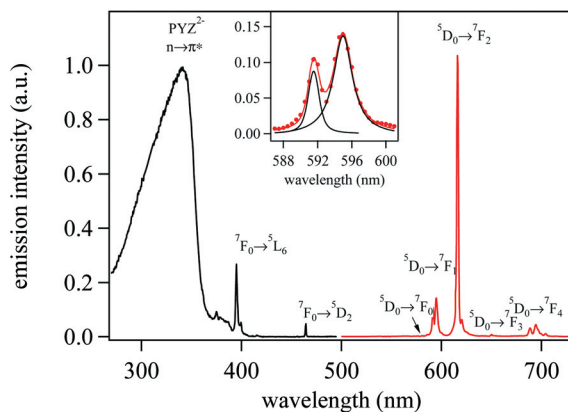

Fig. 4 Solid state excitation (black, λ_{em} = 615 nm) and emission (red, λ_{ex} = 340 nm) spectra of the Cs$_3$[Eu(PYZ)$_3$]·7H$_2$O complex. Inset: expansion of the $^5D_0 \rightarrow {}^7F_1$ emission transition (dotted) at *ca.* 590 nm and fit (red) to two overlapping Voigt functions (black) (see text).

manifold, with observed peak maxima at 591.5, 595 ($J = 1$), 616, 620.5 ($J = 2$), 650 ($J = 3$), and 688.5, 694.5, 704 nm ($J = 4$). Notably, the $J = 0$ transition which was apparent at *ca.* 580 nm in the aqueous solution spectra is now absent (or very weak), which verifies our suggestion that the larger intensity of this peak in aqueous solution originates from the presence of the ML$_2$ complex. Similarly, the $J = 1$ transition is now clearly split into two clearly resolved components, which can be well approximated by overlapping Voigt functions (see inset, Fig. 4). These spectral features are in accordance with those expected[34] for the Eu(III) cation with approximately local D_3 site symmetry, as was observed by X-ray crystallography. The excitation spectrum shows evidence of direct metal-centered absorption bands, with sharp peaks at 395 nm and 464.5 nm which we assign to the $^7F_0 \rightarrow {}^5L_6$ and $^7F_0 \rightarrow {}^5D_2$ transitions respectively. Also present in the spectrum is a broad absorption envelope with a peak maximum at *ca.* 340 nm, which we can again attribute to the principally n → π* transition of the coordinated PYZ^{2-} ligand on the basis of previous reports.[12] Solid-state quantum yield measurements were performed to quantify the observed Eu(III) luminescence intensity, using an integrating sphere method.[10] The resulting value we obtain for Φ_{total} was 60.9 ± 4.6%, which is marginally higher than the value of Φ_{total} = 58 ± 3% reported for the analogous Cs$_3$[Eu(DPA)$_3$]·9H$_2$O complex, although we note that both results are essentially identical within the experimental error. This suggests that ultimately the desired enhancement in Φ_{total} we anticipated by substitution of the DPA^{2-} ligands with PYZ^{2-} was not realised experimentally.

Table 4 Comparison of experimental and calculated luminescence parameters for $Cs_3[Eu(PYZ)_3]\cdot 7H_2O$ and $Cs_3[Eu(DPA)_3]\cdot 9H_2O$ in the solid state (λ_{ex} = 280 nm)

Complex	Φ_{total} (%)	τ_{obs} (ms)	τ_{rad} (ms)	k_{rad} (ms^{-1})	k_{nrad} (ms^{-1})	Φ_{Eu} (%)	η_{sens} (%)
$Cs_3[Eu(PYZ)_3]\cdot 7H_2O$	60.9	1.93	2.66	0.375	0.143	72.4	84.1%
$Cs_3[Eu(DPA)_3]\cdot 9H_2O$	58.0	1.80	2.65	0.378	0.178	66.7	85.3%

The luminescence lifetime of solid $Cs_3[Eu(PYZ)_3]\cdot 7H_2O$ was also measured, yielding a monoexponential decay value of τ_{obs} = 1.93 ± 0.04 ms. Adopting the methodology proposed by Werts et al.[35] and Beeby et al.,[33] and recently verified by Bünzli et al.,[10] we have calculated the radiative lifetime, τ_{rad}, from the corrected emission spectrum of the $Cs_3[Eu(PYZ)_3]\cdot 7H_2O$ complex using the equation:

$$\frac{1}{\tau_{obs}} = A_{MD,0}\eta^3\left(\frac{I_{tot}}{I_{MD}}\right)$$

where η is the refractive index, $A_{MD,0}$ is the emission probability of the $^5D_0 \rightarrow {}^7F_1$ transition (14.65 s^{-1}), and I_{tot} and I_{MD} are the integrated areas of the entire spectrum and the $^5D_0 \rightarrow {}^7F_1$ (MD) transition respectively. The remaining important photophysical parameters, including the intrinsic quantum yield for metal-centered luminescence (e.g. upon direct 4f–4f absorption, or assuming 100% sensitisation efficiency), Φ_{Ln}, can be derived using the following equations:

$$k_{nr} = \frac{1}{\tau_{obs}} - k_r \quad \Phi_{Eu} = \frac{k_r}{(k_r + k_{nr})} \quad \eta_{sens} = \frac{\Phi_{total}}{\Phi_{Eu}}$$

with the resulting values for the $Cs_3[Eu(PYZ)_3]\cdot 7H_2O$ and the $Cs_3[Eu(DPA)_3]\cdot 9H_2O$ complexes summarised and compared in Table 4.

An examination of these photophysical parameters reveals the radiative lifetimes, τ_{rad}, and hence radiative decay rate constants ($k_{rad} = 1/\tau_{rad}$) are quasi-identical for the $Cs_3[Eu(PYZ)_3]\cdot 7H_2O$ and $Cs_3[Eu(DPA)_3]\cdot 9H_2O$ complexes, which can be readily understood since the coordination environment of the Eu(III) cation in both complexes is essentially identical. By contrast, the non-radiative decay rate constant for $Cs_3[Eu(PYZ)_3]\cdot 7H_2O$ is slightly decreased, which we attribute to the loss of three –CH oscillators in close proximity (∼5.2 Å) to the metal centre, since these groups can have a non-radiative quenching effect on metal-centered luminescence.[33] Alternately, the presence of less water in the lattice of $Cs_3[Eu(PYZ)_3]\cdot 7H_2O$, which may otherwise quench Eu(III) luminescence by coupling to νOH vibrations, may also contribute to lower the non-radiative decay rate constant.

As a result of this decrease, the intrinsic metal-centered luminescence quantum yield is enhanced, by ca. 5% relative to $Cs_3[Eu(DPA)_3]\cdot 9H_2O$, but this increase appears to be offset by a lower sensitization efficiency (albeit within the experimental error), resulting in overall quantum yields which are similarly identical within experimental error. Hence, our prediction that the improved efficiency of intersystem crossing observed for the pyrazine vs. pyridine chromophore may lead to more emissive Ln(III) complexes was not upheld experimentally. Rather, it would appear that upon complex formation, the close proximity of the Ln(III) cation has a much stronger influence, enhancing spin orbit coupling (e.g. heavy atom effect) for both complexes,

which likely becomes the most dominant deactivation pathway for the excited singlet state.

Conclusions

We have demonstrated that the tridentate chelate, pyrazine-2,6-dicarboxylic acid (H_2PYZ), is an efficient sensitizer for Eu(III) in the solid state, forming a highly luminescent $Cs_3[Eu(PYZ)_3]\cdot 7H_2O$ complex. In aqueous solution, the isolated compound undergoes partial dissociation below millimolar concentrations, leading to formation of the corresponding hydrolyzed $[Eu(PYZ)_2(H_2O)_3]^{1-}$ and $[Eu(PYZ)(H_2O)_6]^{1+}$ complexes, and resulting in a considerable loss of the overall metal-centered luminescence intensity. In the solid state, the calculated sensitization efficiency, η_{sens}, which can be considered as the product of the intersystem crossing quantum yield, Φ_{isc}, and the efficiency of the energy transfer step, η_{eet}, was found to be quasi-identical to that of a model Eu(III) complex with pyridine-2,6-dicarboxylate, and as a result the luminescence intensity was not significantly altered. This suggests that the dominant relaxation process for the initially formed singlet excited state of these organic chromophores in proximity to Ln(III) cations is most certainly intersystem crossing, with any resulting differences in observed quantum yields being more likely related to the differences in energy transfer efficiencies and the intrinsic metal-centered quantum yield of the luminescent Ln(III) cation. We are currently undertaking ultrafast transient absorption measurements in an attempt to evaluate the influence of these differing antennae structures on the relative intersystem crossing and energy transfer rate constants.

Acknowledgements

References

1 C. P. Montgomery, B. S. Murray, E. J. New, R. Pal and D. Parker, *Acc. Chem. Res.*, 2009, **42**, 925.
2 R. Pal, D. Parker and L. C. Costello, *Org. Biomol. Chem.*, 2009, **7**, 1525.
3 L. N. Krasnoperov, S. A. E. Marras, M. Kozlov, L. Wirpsza and A. Mustaev, *Bioconjugate Chem.*, 2010, **21**, 319.
4 A. Beeby, S. W. Botchway, I. M. Clarkson, S. Faulkner, A. W. Parker, D. Parker and J. A. G. Williams, *J. Photochem. Photobiol., B*, 2000, **57**, 83.
5 A. DAleo, J. Xu, E. G. Moore, C. J. Jocher and K. N. Raymond, *Inorg. Chem.*, 2008, **47**, 6109.

6 S. E. Plush and T. Gunnlaugsson, *Dalton Trans.*, 2008, 3801.
7 G. Nocton, A. Nonat, C. Gateau and M. Mazzanti, *Helv. Chim. Acta*, 2009, **92**, 2257.
8 E. G. Moore, G. Szigethy, J. Xu, L.-O. Palsson, A. Beeby and K. N. Raymond, *Angew. Chem., Int. Ed.*, 2008, **47**, 9500.
9 J. Zhang and S. Petoud, *Chem.–Eur. J.*, 2008, **14**, 1264.
10 (*a*) A. S. Chauvin, F. Gumy, D. Imbert and J-C. G. Bünzli, *Spectrosc. Lett.*, 2004, **37**, 517; (*b*) A. S. Chauvin, F. Gumy, D. Imbert and J-C. G. Bünzli, *Spectrosc. Lett.*, 2007, **40**, 517.
11 A. Aebischer, F. Gumy and J.-C. G. Bünzli, *Phys. Chem. Chem. Phys.*, 2009, **11**, 1346.
12 I. Yamazaki, T. Murao, T. Yamanaka and K. Yoshihara, *Faraday Discuss. Chem. Soc.*, 1983, **75**, 395.
13 F.-Q. Wang, X.-J. Zheng, Y.-H. Wan, C.-Y. Sun, Z.-M. Wang, K.-Z. Wang and L.-P. Jin, *Inorg. Chem.*, 2007, **46**, 2956.
14 F. Weygand, *Chem. Ber.*, 1940, **73**, 1259.
15 H. I. X. Mager and W. Berends, *Recueil*, 1958, **77**, 827.
16 P. A. Brayshaw, J.-C. G. Bünzli, P. Froidevaux, J. M. Harrowfield, Y. Kim and A. N. Sobolev, *Inorg. Chem.*, 1995, **34**, 2068.
17 G. Sheldrick, *SHELX-97 Program for Crystal Structure Solution*, Institüt für Anorganische Chemie der Universität, Gottingen, Germany, 1997.
18 L. J. Farrugia, *J. Appl. Crystallogr.*, 1999, **32**, 837.
19 C. F. Macrae, P. R. Edgington, P. McCabe, E. Pidcock, G. P. Shields, R. Taylor, M. Towler and J. Van de Streek, Mercury: visualization and analysis of crystal structures, *J. Appl. Crystallogr.*, 2006, **39**, 453.
20 J. W. Forrest, *J. Opt. Soc. Am.*, 1942, **32**, 382.
21 G. A. Crosby and J. N. Demas, *J. Phys. Chem.*, 1971, **75**, 991.
22 D. F. Eaton, *Pure Appl. Chem.*, 1988, **60**, 1107.
23 P. Gans and B. O'Sullivan, *Talanta*, 2000, **51**, 33.
24 P. Gans, A. Sabatini and A. Vacca, *Talanta*, 1996, **43**, 1739.
25 J.-C. G. Bünzli, J. R. Yersin and C. Mabillard, *Inorg. Chem.*, 1982, **21**, 1471.
26 C. F. Baes and R. E. Mesmer, *The Hydrolysis of Cations*, Wiley-Interscience, New York, 1976.
27 W. D. W. Horrocks and D. R. Sudnick, *J. Am. Chem. Soc.*, 1979, **101**, 334.
28 C. J. Lewis, *J. Biol. Chem.*, 1972, **247**, 1861.
29 I. Grenthe, *J. Am. Chem. Soc.*, 1961, **83**, 360.
30 R. M. Tichane and W. E. Bennett, *J. Am. Chem. Soc.*, 1957, **79**, 1293.
31 M. Heitzmann, F. Bravard, C. Gateau, N. Boubals, C. Berthon, J. Pecaut, M.-C. Charbonnel and P. Delangle, *Inorg. Chem.*, 2009, **48**, 246.
32 J.-C. G. Bunzli, Luminescent probes, in *Lanthanide Probes in Life, Chemical and Earth Sciences: Theory and Practice*, ed. J.-C. G. Bunzli and G. R. Choppin, Elsevier, Amsterdam, 1989.
33 A. Beeby, L. M. Bushby, D. Maffeo and J. A. G. Williams, *J. Chem. Soc., Dalton Trans.*, 2002, 48.
34 G. M. Murray, R. V. Sarrio and J. R. Peterson, *Inorg. Chim. Acta*, 1990, **176**, 233.
35 M. H. V. Werts, R. T. F. Jukes and J. W. Verhoeven, *Phys. Chem. Chem. Phys.*, 2002, **4**, 1542.